



1 Significant contributions of biomass burning to PM_{2.5}-bound aromatic
2 compounds: insights from field observations and quantum chemical
3 calculations

4
5 Yanqin Ren¹, Zhenhai Wu¹, Fang Bi¹, Hong Li¹, Haijie Zhang^{1*}, Junling Li¹, Rui Gao¹,
6 Fangyun Long¹, Zhengyang Liu¹, Yuanyuan Ji^{1*}, Gehui Wang^{2*}

7

8 ¹ State Key Laboratory of Environmental Criteria and Risk Assessment, Chinese
9 Research Academy of Environmental Sciences, Beijing 100012, China

10 ² Key Lab of Geographic Information Science of Ministry of Education of China,
11 School of Geographic Sciences, East China Normal University, Shanghai 200142,
12 China

13

14

15 *Corresponding authors: Dr. Haijie Zhang /Dr. Yuanyuan Ji/ Prof. Gehui Wang

16 E-mail address: zhanghaijie@craes.org.cn / ji.yuanyuan@craes.org.cn

17 / ghwang@geo.ecnu.edu.cn

18



19 **Abstract**

20 Polycyclic aromatic hydrocarbons (PAHs), oxygenated PAHs (OPAHs), and
21 nitrated phenols (NPs) are essential aromatic compounds that significantly affect both
22 climate and human health. However, their sources and formation mechanisms,
23 particularly for NPs, remain poorly understood. This study determined the
24 concentration profiles and the main formation mechanisms of these substance classes
25 in PM_{2.5} from Dongying, based on field observations and quantum chemical
26 calculations. The daily concentrations of $\Sigma 13$ PAHs during heating were more than
27 twice higher compared to those before the heating period. Benzo(*b*)fluoranthene was
28 identified as the primary PAHs species. The average concentration of $\Sigma 8$ OPAHs
29 reached 351 ng m⁻³, with significantly increased concentrations observed during the
30 heating season, and 1-Naphthaldehyde (1-NapA) emerged as the most prevalent OPAH
31 species. Concentrations of $\Sigma 9$ NPs increased approximately 1.2 times during the heating,
32 with 4-methyl-5-nitrocatechol (4M5NC) having the highest concentration. Positive
33 matrix factorization analysis identified biomass burning to be the primary source of
34 these aromatic compounds, particularly for PAHs. Density functional theory
35 calculations further revealed that phenol and nitrobenzene are two main primary
36 precursors for 4-nitrophenol, with phenol showing lower reaction barriers, and *P*-Cresol
37 was identified as the primary precursor for the formation of 4M5NC. This study
38 provides the first detailed investigation of the sources and formation mechanisms of
39 aromatic compounds in the atmosphere of petrochemical cities in the Yellow River
40 Delta, which may provide fundamental insights and important guidance for reducing



41 emissions of aromatic compounds in similar atmospheric environments.

42

43 **Keywords:** Aromatic compounds, Source identification, DFT calculations, Formation

44 mechanism, Heating period

45 **1. Introduction**

46 Aromatic compounds, characterized by the presence benzene ring, are known for
47 their structural stability and resistance to decomposition, as well as their distinctive
48 aromatic properties. Polycyclic aromatic hydrocarbons (PAHs), oxygenated PAHs
49 (OPAHs), and nitrated phenols (NPs) are significant aromatic compounds commonly
50 found in atmospheric particulate matter. These compounds exerted a considerable
51 influence on ambient air quality, climate change, and human health (Peng et al., 2023;
52 Yhab et al., 2021; Chong et al., 2021; Lammel et al., 2020; Elzein et al., 2019).

53 PAHs are semi-volatile compounds, comprised of multiple interconnected
54 aromatic rings and are commonly found throughout various environmental settings.
55 PAHs are primarily formed as byproducts of the partial combustion of carbon-rich
56 substances, including coal, biomass, tobacco, garbage, charbroiled meat, and petroleum
57 (Del Rosario Sienna et al., 2005; Kashiwakura and Sakamoto, 2010; Chen et al., 2005;
58 Shen et al., 2010). OPAHs are aromatic compounds with one or more carbonyl groups
59 connected to their ring structure, and they contain various quinones and ketones.
60 OPAHs generally have lower vapor pressures upon comparison with their parent PAHs,
61 leading to a higher propensity to be retained in the particulate phase. The direct-acting



62 mutagen properties and the generation of reactive O₂ species render some OPAHs more
63 hazardous compared with the parent PAHs (Bandowe et al., 2010; Chung et al., 2006;
64 Bolton et al., 2000; Pedersen et al., 2005). OPAHs is carried out either directly through
65 the incomplete combustion of various organic materials (Oda et al., 2001; Jakober et
66 al., 2007) or can be formed indirectly through photochemical reactions involving PAHs
67 and ozone, nitro, and hydroxyl radicals (Bandowe et al., 2014; Wang et al., 2011; Lin
68 et al., 2015b). Research suggests that the PAH concentrations, along with their
69 derivatives in PM_{2.5}, increased during winter or heating periods, primarily due to
70 biomass and coal burning (Lin et al., 2015b). Furthermore, particulate matter released
71 from biomass burning is considered more toxic compared to that derived from other
72 sources (Sarigiannis et al., 2015). NPs are monocyclic aromatic compounds having
73 properties similar to benzene, including low solubility in water while high solubility in
74 various organic solvents such as ethanol, pyridine, xylene, and chloroform. In addition
75 to adversely affecting human health, NPs can also disrupt the equilibrium of the
76 ecosystem, increase the risk of cancer, and disrupt plant growth (Chow et al., 2015;
77 Liang et al., 2020; Booth et al., 2014). NPs in the atmosphere are primarily derived
78 from primary emissions and secondary formation. Primary sources of NPs include
79 emissions from coal combustion, vehicle exhaust, biomass combustion, and industrial
80 and agricultural sources, similar to the sources of PAHs and OPAHs (Liang et al., 2020;
81 Wang et al., 2017; Lu et al., 2021). Observations in the atmospheric environment
82 indicate that secondary formation can provide more than one-third of the total NPs
83 present (Yuan et al., 2016a). Benzene, toluene, and their derivatives are considered



84 significant precursors in the secondary formation of NPs, although secondary NPs can
85 also be generated through nitrification of phenols in the gas or condensation phase or
86 by interactions between phenoxy radicals, formed from NO₂, and other aromatic
87 compounds (Harrison et al., 2005).

88 In Dongying City, known for its petrochemical industry, benzene, toluene, and
89 xylene are significant contributors to the levels of VOCs into the environment (Chen et
90 al., 2020). Moreover, research has revealed that in the presence of NO_x, aromatic
91 hydrocarbons can be oxidized to yield nitroaromatic compounds, including nitrophenol,
92 dinitrophenol, nitrocatechol, and methylnitrocatechol (Lin et al., 2015a). The primary
93 sources of aromatic compounds in particulate matter within high-aromatic
94 environments and the potential relationship between their secondary formation and the
95 benzene series mentioned earlier still require systematic investigation. Therefore, this
96 study explored the pollution characteristics and primary sources of PAHs, OPAHs, and
97 NPs in PM_{2.5} in Dongying City, and further explored the formation mechanism of
98 typical nitrophenols based on field observations and density functional theory
99 calculations. This study represents the first investigation regarding the sources and the
100 forming mechanisms of aromatic compounds within the atmosphere of petrochemical
101 cities in the Yellow River Delta.

102 **2 Materials and Methods**

103 **2.1 Field observations**

104 PM_{2.5} samples collection was carried out at Dongying Atmospheric Super Station



105 (118.59°E, 37.45°N) from October 27 to December 6, 2021. The surrounding area is
106 primarily residential and commercial, with well-developed transportation infrastructure
107 and no significant sources of industrial pollution, making it a representative urban
108 monitoring site. A high-flow particulate sampler (TH-1000H, Wuhan Tianhong
109 Instrument Co., LTD) was employed to obtain the samples. This instrument had a
110 sampling flow rate equal to 1.05 m³/min and a flow accuracy of ±2.5%. It comprised a
111 quartz filter (Quartz, 203 mm×254 mm, Whatman, UK), with an effective filter
112 diameter of 180 mm×230 mm. Samples were collected twice daily: once during the day
113 from 8:00 am to 7:30 pm local time (LT) and once from 8:00 pm to 7:30 am LT.
114 Meteorological statistics, including temperature, weather conditions, humidity, wind
115 direction and speed, were measured concurrently with each sampling.

116 **2.2 Chemical analysis**

117 Organic species in PM_{2.5} were detected following a pre-treatment process that
118 included ultrasonic extraction along with derivatization. Initially, a quarter of the
119 membrane was placed into a sample bottle and then immersed in a mixture of
120 dichloromethane and methanol solution (2:1, v/v) to completely submerge the filters.
121 After that, three 15-min treatments of ultrasonic extraction were carried out. Following
122 the process of extraction, filtration was carried out through glass wool using a Babbitt
123 dropper into pear-shaped flasks. The filtrates were then concentrated to a small amount
124 through a rotary evaporator inside a vacuum. Subsequently, they were transferred to
125 GC bottles, which were dried with a nitrogen purifier, followed by the addition of 60
126 μL of N, O-bis-(trimethylsilyl) trifluoroacetamide solution. The bottles were then



127 placed in an oven at 70 °C for a total time duration of 3 h to complete the derivatization
128 process. After the reaction, the solution was cooled and an internal standard comprised
129 of 40 µL tridecane was added. The solution was mixed completely and then placed in
130 the refrigerator for examination.

131 This study analyzed thirteen different PAHs, eight different OPAHs, and nine
132 different NPs using the afore mentioned methods of analysis, as well as some organic
133 tracers, e.g. levoglucosan. The thirteen kinds of PAHs include Fluoranthene (Flu),
134 Benzo[k]fluoranthene (BkF), Benzo[a]anthracene (BaA), Pyrene (Pyr),
135 Chrysene/triphenylene(CT), Benzo[b]fluoranthene (BbF), Benzo[a]pyrene (BaP),
136 Benzo[e]pyrene (BeP), Indeno[1,2,3-cd] (IP), Perylene (Per), Benzo[ghi]perylene
137 (BghiP), Dibenzo[a,h]anthracene (DBA), and Coronene. The eight OPAHs include
138 benzanthrone (BZA), 9-fluorenone (9-FO), 1-Naphthaldehyde (1-NapA), 1,4-
139 chrysenequinone (1,4-CQ), anthraquinone (ATQ), 5,12-naphthacenequinone (5,12-NAQ),
140 benzo(a)anthracene-7,12-dione (7,12-BaAQ), and 6H-benzo(cd)pyrene-6-one
141 (BPYRone). The nine NPs are 4-nitrophenol (4NP), 4-nitroguaiacol (4NGA), 3-methyl-
142 4-nitrophenol (3M4NC), 4-methyl-5-nitrocatechol (4M5NC), 4-nitrocatechol (4NC),
143 5-nitroguaiacol (5NGA), 2, 4-dinitrophenol (2, 4-DNP), 5-nitro-salicylic acid (5NSA)
144 and 3-nitro-salicylic acid (3NSA).

145 Inorganic ions soluble in water were quantified through an ion chromatograph
146 (Dionex-1100). The analysis focused on eight water-soluble inorganic ions: NO₃⁻, Cl⁻,
147 NH₄⁺, SO₄²⁻, Na⁺, Mg²⁺, K⁺, and Ca²⁺. The measurement of organic carbon (OC) and
148 elemental carbon (EC) was performed through a thermal/optical carbon analyzer



149 (DRI2015). Detailed tests for analyzing EC, OC, and inorganic ions are provided in a
150 previous report (Ren et al., 2021).

151 **2.3 Quantum chemical calculations**

152 Quantum chemical calculations both in the gas phase and liquid phase were
153 performed using the Gaussian 09 software. The geometries and frequencies for the
154 reactant monomers, reactant complexes (RC), transition states (TS), intermediate (IM)
155 and product complexes (PC) were performed at the M06-2X/6-311++G(2df,2p) level
156 of theory, which is well-established for studies of organic systems (Li and Wang,
157 2014; Zhao and Truhlar, 2007). The conductor-like polarizable continuum
158 model(CPCM) was used for the optimization calculations to include the solvent effect
159 in the liquid (Takano and Houk, 2005). Radicals were treated using unrestricted
160 Hartree–Fock calculations, and TS was optimized to ensure the presence of a single
161 imaginary frequency. Intrinsic reaction coordinate (IRC) calculations were carried out
162 to further guarantee that the TS connects the right pre- and post-complexes along the
163 reaction coordinate (Gonzalez and Schlegel, 1989).

164 **2.4 Quality control and quality assurance (QC&QA)**

165 QA and QC procedures for sampling and laboratory analysis strictly follow the
166 environmental monitoring technical specifications and analytical standards established
167 by the Ministry of Environmental Protection. Periodic inspections of all analytical and
168 testing instruments were carried out in accordance with the relevant metrological
169 verification protocols. The quartz filter membrane was burned inside a Muffle furnace
170 at a temperature of 450 °C for 6 h before sampling. After natural cooling, it was



171 removed and transferred to a controlled temperature and humidity box (25 ± 1 °C, $50 \pm$
172 5% RH). The sampled filter membrane was packed in a ziplock bag and stored in the
173 refrigerator at a temperature below 0 °C until analysis. To minimize systematic errors,
174 corresponding blank filter samples were simultaneously prepared and stored followed
175 by analysis under the same conditions as the collected samples.

176 **3 Results and discussion**

177 **3.1 Changes in meteorological conditions, gaseous pollution, and major** 178 **components of PM_{2.5}**

179 The entire study period was divided into two stages: before heating (October 27 to
180 November 14, 2021) and during heating (November 15 to December 6, 2021). Fig. 1
181 and Table 1 illustrate the temporal variations within the meteorological factors,
182 concentrations of gaseous pollutants, as well as the primary components of PM_{2.5}.
183 Before heating, the relative humidity (RH) and temperature (T) were higher, averaging
184 $64 \pm 18\%$ and 12 ± 5.4 °C, respectively. During the heating period, the average values
185 were found to be lower at $60 \pm 18\%$ and 7.9 ± 3.7 °C. Overall, the average values for
186 the entire study period were determined to be $62 \pm 18\%$ and 9.6 ± 4.9 °C. The
187 concentrations of SO₂ and NO during heating (11 ± 6.6 ppb, and 17 ± 16 ppb,
188 respectively) were nearly twice that of the value observed before heating, with a slight
189 increase in the level of NO₂. These increases are likely attributable to the increased
190 burning activities during the heating season, particularly residential coal combustion.
191 In contrast, the levels of O₃ and O_x (the sum of NO₂ and O₃) were significantly higher



192 before heating, with an average value of 49 ± 27 ppb and 80 ± 28 ppb, respectively, in
193 comparison to that observed during the heating period. This variation was primarily
194 ascribed to the higher temperatures and stronger solar radiation before heating.

195 Although the $PM_{2.5}$ concentrations remained unchanged throughout the sampling
196 period, there were considerable variations in the concentrations and proportions of its
197 chemical components. Figs.1 and 2 showed the time variations and absolute proportion
198 of chemical components in $PM_{2.5}$ before and during heating, respectively, throughout
199 the entire sampling period. Throughout the observation period, secondary inorganic
200 aerosols (SIA) such as SO_4^{2-} , NO_3^- , and NH_4^+ were determined as the main chemical
201 component of $PM_{2.5}$, followed by OM (1.6 times the OC). Before heating, the
202 concentrations of SO_4^{2-} , NO_3^- , and NH_4^+ were found to be 5.5, 17, and $7.5 \mu g m^{-3}$,
203 respectively, while during heating, they demonstrated the average values of 5.3, 17, and
204 $7.7 \mu g m^{-3}$ (Fig. 1b, c). The total concentrations and proportions of SIA remained
205 relatively stable, with an average of about 35% during the whole process. Among these,
206 NO_3^- was determined as the predominant species, constituting approximately 19% of
207 the total $PM_{2.5}$ during the sampling period. OM comprised 12.7% of $PM_{2.5}$ before the
208 heating period and increased significantly to 17.5% during heating (Fig. 2b, c).
209 Correspondingly, the average OC concentration increased from 5.4 to $7.7 \mu g m^{-3}$.
210 However, the average ratio of OC/EC remained relatively unchanged, with values of
211 2.5 ± 1.1 before heating and 2.4 ± 0.6 during heating. Generally, OC is generated from
212 both primary emissions and secondary formation, while EC is predominantly derived
213 from primary sources. The significant increase in the concentration of OC alongside a



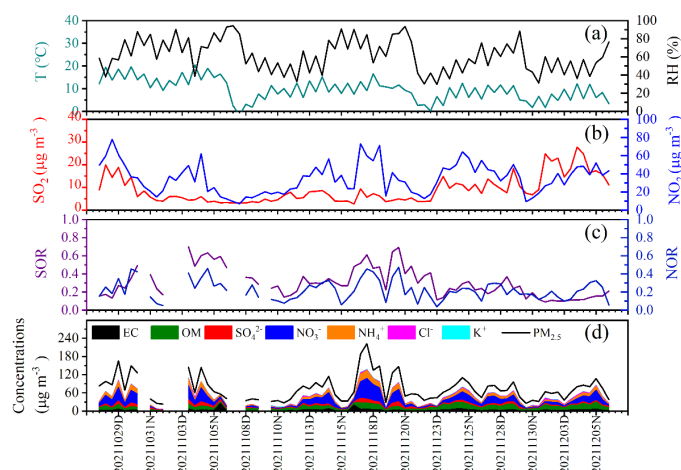
214 stable OC/EC ratio suggests that the sources of carbonaceous aerosols in this study
 215 include both primary emissions and secondary formation processes. Furthermore, a
 216 high positive correlation between levoglucosan and K⁺ and Cl⁻ (Fig. 3), along with the
 217 enhanced mass concentrations of these ions during the heating period, suggests
 218 additional combustion activities, including biomass burning, in addition to coal
 219 combustion.

Table 1. Meteorological parameter values and concentrations of gaseous pollution and chemical components of PM_{2.5} during the sampling periods in Dongying.

Period	The whole sampling	Before heating period	During heating period
Date	27/10–6/12	27/10–14/11	15/11–6/12
Scope of the Sample	N=74	N=30	N=44
Meteorological parameters			
Temperature, °C	9.6 ± 4.9 ((-1.7) – 21)	12 ± 5.4 ((-1.7) – 21)	7.9 ± 3.7 (0.2 – 17)
Relative humidity, %	62 ± 18 (29 – 94)	64 ± 18 (33 – 95)	60 ± 18 (30 – 94)
Gaseous pollutants, ppb			
SO ₂	8.9 ± 5.9 (2.7 – 28)	6.7 ± 4.2 (3.1 – 20)	11 ± 6.6 (2.7 – 28)
NO	13 ± 14 (NA – 54)	8.5 ± 11 (0.2 – 41)	17 ± 16 (1.0 – 54)
NO ₂	35 ± 17 (6.8 – 78)	32 ± 18 (6.8 – 78)	38 ± 16 (9.2 – 73)
O ₃	39 ± 23 (3.8 – 106)	49 ± 27 (3.8 – 106)	30 ± 16 (8.9 – 83)
O _x	74 ± 25 (43 – 167)	80 ± 28 (51 – 167)	68 ± 20 (43 – 137)
Major components of PM_{2.5}, µg m⁻³			
PM _{2.5}	74 ± 42 (23 – 222)	74 ± 41 (23 – 167)	75 ± 43 (25 – 222)
OC	6.8 ± 3.5 (0.6 – 15)	5.4 ± 2.7 (0.6 – 10)	7.7 ± 3.8 (1.4 – 15)
EC	3.7 ± 3.8 (0.2 – 26)	3.5 ± 4.7 (0.2 – 26)	3.8 ± 3.2 (0.6 – 20)
OC/EC	2.4 ± 0.8 (0.1 – 5.1)	2.5 ± 1.1 (0.1 – 5.1)	2.4 ± 0.6 (0.2 – 3.6)
SO ₄ ²⁻	5.4 ± 3.5 (1.2 – 17)	5.5 ± 3.6 (1.2 – 15)	5.3 ± 3.4 (1.5 – 17)
NO ₃ ⁻	17 ± 15 (1.5 – 67)	17 ± 15 (1.5 – 46)	17 ± 16 (1.6 – 67)
NH ₄ ⁺	7.6 ± 6.1 (0.6 – 27)	7.5 ± 6.1 (0.9 – 21)	7.7 ± 6.2 (0.6 – 27)
Cl ⁻	1.8 ± 1.2 (0.2 – 6.1)	1.5 ± 1.3 (0.2 – 6.1)	2.0 ± 1.1 (0.5 – 5.3)
K ⁺	0.6 ± 0.4 (0.1 – 2.0)	0.5 ± 0.4 (0.1 – 2.0)	0.6 ± 0.3 (0.1 – 1.2)

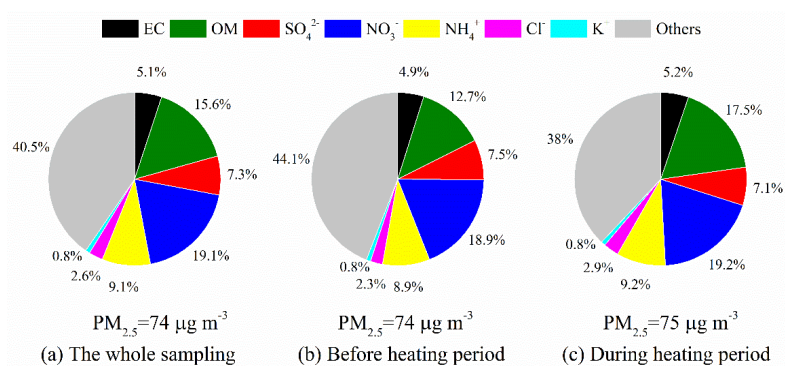
220

221



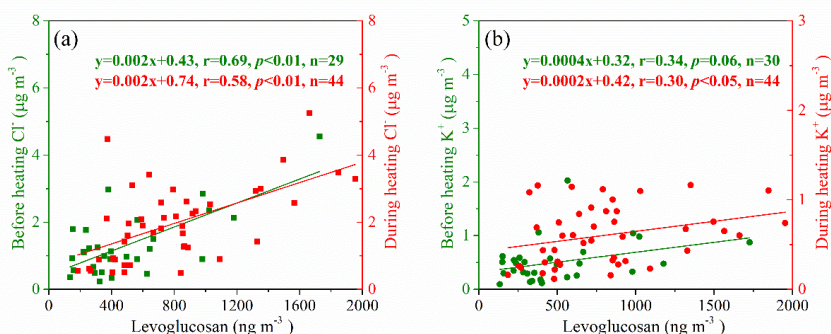
222
223
224
225

Fig.1 Time series of (a) T and RH, (b) NO₂ and SO₂, (c) SOR and NOR, and (d) PM_{2.5} and its main compounds, in the winter and autumn of Dongying.



226

Fig.2 Absolute proportion of chemical components in PM_{2.5} across the whole sampling period (a), before (b), and during the heating periods (c).



229
230
231
232

Fig.3 Regression analysis showing the linear relationship between levoglucosan and Cl⁻ (a) and K⁺ (b) before (green) and during (red) heating throughout the sampling period.



233 3.2 Changes in the concentration and composition of aromatic compounds

234 3.2.1 PAHs and OPAHs

235 Table 2 and Fig. 4b show that the daily concentrations of 13 different PAHs (Σ
236 13PAHs) ranged from 3.9 to 388 $\text{ng}\cdot\text{m}^{-3}$, with 91 $\text{ng}\cdot\text{m}^{-3}$ of overall average value
237 throughout the sampling period. During the heating phase, concentrations averaged 115
238 $\text{ng}\cdot\text{m}^{-3}$ (over a range of 15 to 388 $\text{ng}\cdot\text{m}^{-3}$), more than twice the levels recorded before
239 heating, which averaged 56 $\text{ng}\cdot\text{m}^{-3}$ (over a range of 3.9 to 241 $\text{ng}\cdot\text{m}^{-3}$). The Σ 13 PAHs
240 measured in the current research were lower in comparison to those recorded in other
241 Chinese cities, including Xi 'an (127 $\text{ng}\cdot\text{m}^{-3}$, 2016–2017) (Wang et al., 2019a) and
242 Harbin (215 $\text{ng}\cdot\text{m}^{-3}$, 2017–2018) (Ma et al., 2020). Nighttime average concentrations
243 of PAHs ($65 \pm 77 \text{ ng}\cdot\text{m}^{-3}$ before heating and $154 \pm 120 \text{ ng}\cdot\text{m}^{-3}$ during heating) were
244 observed to be 1.5 to 2 times higher upon comparison with those measured during the
245 daytime ($44 \pm 39 \text{ ng}\cdot\text{m}^{-3}$ before heating and $77 \pm 49 \text{ ng}\cdot\text{m}^{-3}$ during heating) (Fig. 5a).
246 The observed day-night pattern aligns with the observations obtained from coastal cities
247 in Bohai and the Yellow Seas, as well as Jinan in Shandong Province (Chen et al., 2021;
248 Zhang et al., 2018). The concentration level of BbF in PAHs was found to be highest,
249 accounting 16% of total PAHs (Fig. 4b), This dominance of BbF was found to be
250 consistent with the previous research (Li et al., 2013; Ren et al., 2017; Bai et al., 2023;
251 Li et al., 2022).

252 The average total concentration of OPAHs (Σ 8OPAHs) was determined to be 351
253 $\text{ng}\cdot\text{m}^{-3}$ across all the sampling periods, which was substantially higher during the
254 heating period (average 378 $\text{ng}\cdot\text{m}^{-3}$, range 114–812 $\text{ng}\cdot\text{m}^{-3}$) compared to the period of



255 before heating (average $311 \text{ ng}\cdot\text{m}^{-3}$, range $70\text{--}875 \text{ ng}\cdot\text{m}^{-3}$) (Table 2). The concentration
256 of $\sum 8\text{OPAHs}$ was higher at night upon comparison with daytime, being approximately
257 1.1 to 1.2 times greater both before and during the heating period (Fig. 4c and 5b).
258 Among the eight OPAHs, 1-NapA was determined as the most prevalent, accounting
259 for 187 ng m^{-3} (59% of $\sum 8\text{OPAHs}$) before heating and 156 ng m^{-3} (41% of $\sum 8\text{OPAHs}$)
260 during heating (Fig. 4c and 5e). The average $\sum 8\text{OPAHs}$ concentrations in this study
261 were significantly higher compared with those found for other Chinese urban areas,
262 such as Guangzhou and Xi'an, with respective values of 23 and 54 ng m^{-3} (Ren et al.,
263 2017). Furthermore, the $\sum 8\text{OPAHs}$ levels observed in this study exceeded those
264 reported at various foreign sites, such as the south (traffic site, 41.8 ng m^{-3}) (Alves et
265 al., 2017) and central European cities (about 10 ng m^{-3}) (Lammel et al., 2020),
266 Thessaloniki, Greece ($0.86\text{--}4.3 \text{ ng m}^{-3}$) (Kitanovski et al., 2020), and Mainz, Germany
267 ($0.047\text{--}1.6 \text{ ng m}^{-3}$).

268 **3.2.2 NPs**

269 Based on the data presented in Table 2, the total concentrations of NPs compounds
270 ($\sum 9\text{NPs}$) demonstrated a mean value equal to 72 ng m^{-3} across the sampling period.
271 During the heating phase, $\sum 9\text{NPs}$ averaged 76 ng m^{-3} (covering a range extending from
272 23 to 175 ng m^{-3}), which was approximately 1.2 times higher compared to the
273 concentrations determined before heating, with an average of 65 ng m^{-3} (covering a
274 range of 4.2 to 149 ng m^{-3}). These concentrations were approximately twice those
275 observed during autumn and winter (38 ng m^{-3}) in earlier work conducted in Beijing



276 (Ren et al., 2024). They were also considerably higher in comparison to the values
277 recorded in the summer (8.5 ng m^{-3}) and spring (8.6 ng m^{-3}) (Ren et al., 2022). In
278 contrast to OPAHs and PAHs, the total concentrations of $\Sigma 9\text{NPs}$ did not demonstrate
279 significant diurnal variation. However, during the heating period, a significant
280 nighttime increase was observed, with approximately 1.4 times higher concentrations
281 at night upon comparison with the levels of daytime (Fig. 4d and Fig. 5c). However,
282 the relative nine NPs molecular composition in $\text{PM}_{2.5}$ remained consistent throughout
283 the observation period. Among all the species, 4M5NC demonstrated the highest
284 concentration, contributing to 73% of the total NPs before heating and 53% during
285 heating, followed by 4NP, comprising 20% before heating and increased to 34% during
286 heating (Fig.4d and Fig. 5f). The total concentration of $\Sigma 9\text{NPs}$ observed in the current
287 research was generally comparable to previous measurements carried out in Beijing
288 during winter ($74 \pm 51 \text{ ng m}^{-3}$) (Li et al., 2020). Conversely, the levels were substantially
289 higher compared to those recorded in Jinan ($48 \pm 26 \text{ ng m}^{-3}$) (Wang et al., 2018), Hong
290 Kong, and Xi'an, with respective values of 12 ± 14 and $17 \pm 12 \text{ ng m}^{-3}$ (Wu et al., 2020;
291 Chow et al., 2015). Compared to the international research, the observed $\Sigma 9\text{NPs}$
292 concentrations were generally higher, such as those reported in Germany (16 ng m^{-3}),
293 the UK (19 ng m^{-3}), and Belgium (32 ng m^{-3} in winter, 13 ng m^{-3} in autumn) (Teich et
294 al., 2017; Mohr et al., 2013; Kahnt et al., 2013).

Table 2. Organic compounds in $\text{PM}_{2.5}$ during the sampling periods in Dongying.

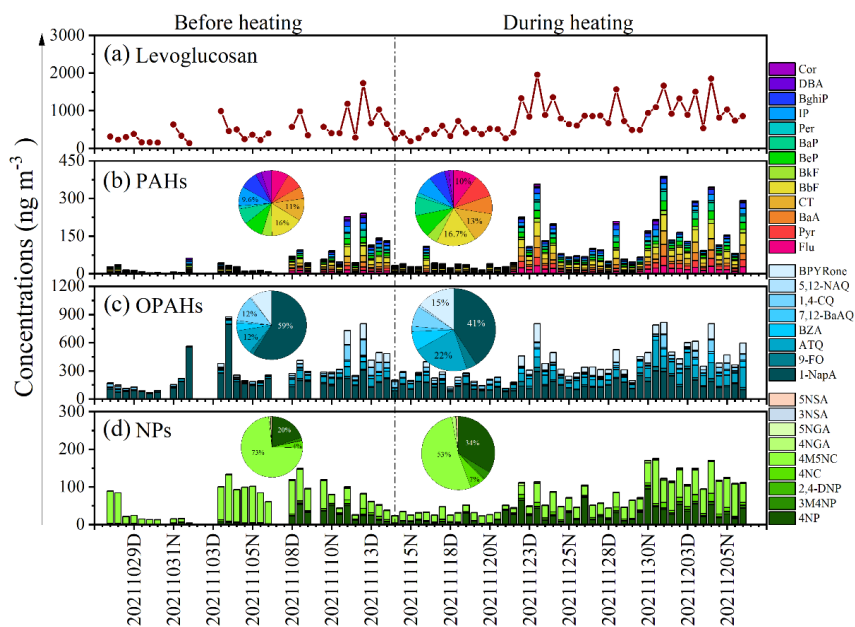
Period	The whole sampling	Before heating period	During heating period
Date	27/10–6/12	27/10–14/11	15/11–6/12
Scope of the Sample	$N=74$	$N=30$	$N=44$
PAHs			



Fluoranthene (Flu)	8.9 ± 8.1 (0.8 – 33)	5.0 ± 4.3 (0.8 – 15)	12 ± 9.0 (1.7 – 33)
Pyrene (Pyr)	8.5 ± 8.4 (0.7 – 36)	4.7 ± 4.3 (0.7 – 16)	11 ± 9.5 (1.4 – 36)
benz(a)anthracene (BaA)	6.8 ± 9.3 (0.1 – 47)	3.5 ± 4.5 (0.1 – 20)	9.0 ± 11 (0.7 – 47)
chrysene/triphenylene (CT)	11 ± 12 (0.7 – 54)	6.4 ± 6.7 (0.7 – 26)	15 ± 13 (1.9 – 54)
benzo(b)fluoranthene (BbF)	15 ± 15 (0.5 – 64)	9.2 ± 10 (0.5 – 39)	19 ± 16 (3.0 – 64)
benzo(k)fluoranthene (BkF)	4.4 ± 4.0 (0.2 – 17)	2.9 ± 2.8 (0.2 – 11)	5.4 ± 4.4 (0.8 – 17)
benzo(e)pyrene (BeP)	9.0 ± 8.5 (0.4 – 37)	5.5 ± 6.1 (0.4 – 24)	11 ± 9.1 (1.8 – 37)
benzo(a)pyrene (BaP)	7.5 ± 8.7 (0.1 – 38)	4.5 ± 6.0 (0.1 – 25)	9.5 ± 9.7 (0.9 – 38)
Perylene (Per)	1.6 ± 2.1 (0.01 – 10)	0.9 ± 1.4 (0.01 – 57)	2.0 ± 2.4 (0.2 – 9.6)
indeno(1,2,3-cd)pyrene (IP)	7.6 ± 7.2 (0.1 – 26)	5.5 ± 6.7 (0.01 – 24)	8.8 ± 7.3 (0.8 – 26)
benzo(ghi)perylene (BghiP)	6.8 ± 6.4 (0.1 – 23)	5.0 ± 6.1 (0.02 – 23)	7.9 ± 6.4 (0.9 – 23)
dibenz(a,h)anthracene (DBA)	1.9 ± 2.4 (0.01 – 15)	1.7 ± 2.1 (0.01 – 7.8)	2.0 ± 2.5 (0.1 – 15)
coronene	2.5 ± 2.6 (0.05 – 11)	2.9 ± 3.6 (0.05 – 11)	2.4 ± 2.2 (0.1 – 9.0)
Σ13PAHs	91 ± 90 (3.9 – 388)	56 ± 62 (3.9 – 241)	115 ± 98 (15 – 388)
OPAHs			
1-naphthaldehyde (1-NapA)	168 ± 106 (57 – 796)	187 ± 149 (57 – 796)	156 ± 62 (75 – 320)
9-fluorenone (9-FO)	12 ± 12 (0.2 – 47)	6.6 ± 7.1 (0.2 – 22)	16 ± 13 (1.0 – 47)
anthraquinone (ATQ)	64 ± 50 (1.1 – 282)	37 ± 29 (1.1 – 103)	83 ± 53 (10 – 282)
benzathrone (BZA)	22 ± 22 (0.2 – 95)	12 ± 15 (0.2 – 58)	29 ± 24 (2.8 – 95)
benzo(a)anthracene-7,12-dione (7,12-BaAQ)	6.3 ± 5.3 (0.5 – 24)	3.8 ± 3.9 (0.5 – 16)	7.9 ± 5.4 (1.3 – 24)
1,4-chrysenequione (1,4-CQ)	34 ± 34 (2.0 – 168)	39 ± 41 (9.2 – 168)	30 ± 28 (2.0 – 136)
5,12-naphthacenequione (5,12-NAQ)	2.6 ± 2.4 (0.02 – 9.4)	1.6 ± 2.1 (0.2 – 8.1)	3.2 ± 2.4 (0.5 – 9.4)
6H-benzo(cd)pyrene-6-one (BPYRone)	47 ± 46 (0.5 – 196)	32 ± 45 (0.5 – 166)	57 ± 45 (4.7 – 196)
Σ8OPAHs	351 ± 196 (70 – 875)	311 ± 209 (70 – 875)	378 ± 185 (114 – 815)
NPs			
4-nitrophenol (4NP)	21 ± 20 (0.4 – 95)	13 ± 16 (0.42 – 54)	26 ± 21 (1.8 – 95)
3-methyl-4-nitrophenol (3M4NP)	2.0 ± 2.0 (0.04 – 7.8)	1.0 ± 1.3 (0.04 – 4.8)	2.6 ± 2.2 (0.16 – 7.8)
4-nitroguaiacol (4NGA)	1.0 ± 1.4 (0.02 – 7.5)	0.5 ± 0.8 (0.02 – 2.9)	1.4 ± 1.6 (0.04 – 7.5)
5-nitroguaiacol (5NGA)	0.09 ± 0.07 (0.01 – 0.3)	0.12 ± 0.07 (0.01 – 0.3)	0.07 ± 0.06 (0.01 – 0.22)
4-nitrocatechol (4NC)	4.1 ± 4.4 (0.1 – 21)	2.6 ± 3.5 (0.1 – 16)	5.0 ± 4.7 (0.39 – 21)
2,4-dinitrophenol (2,4-DNP)	0.24 ± 0.29 (0.004 – 1.3)	0.14 ± 0.22 (0.004 – 0.92)	0.31 ± 0.31 (0.006 – 1.3)
4-methyl-5-nitrocatechol (4M5NC)	48 ± 49 (8.7 – 385)	49 ± 35 (8.7 – 125)	40 ± 25 (8.9 – 116)
3-nitrosalicylic acid (3NSA)	0.03 ± 0.03 (NA – 0.17)	0.03 ± 0.03 (0.003 – 0.17)	0.03 ± 0.03 (0.01 – 0.13)
3-nitrosalicylic acid (5NSA)	0.63 ± 0.45 (0.07 – 1.8)	0.48 ± 0.40 (0.07 – 1.8)	0.72 ± 0.46 (0.07 – 1.8)
Σ9NPs	72 ± 44 (4.2 – 175)	65 ± 42 (4.2 – 149)	76 ± 45 (23 – 175)
Levoglucosan	679 ± 431 (134 – 1954)	497 ± 362 (134 – 1727)	803 ± 433 (185 – 1954)



295



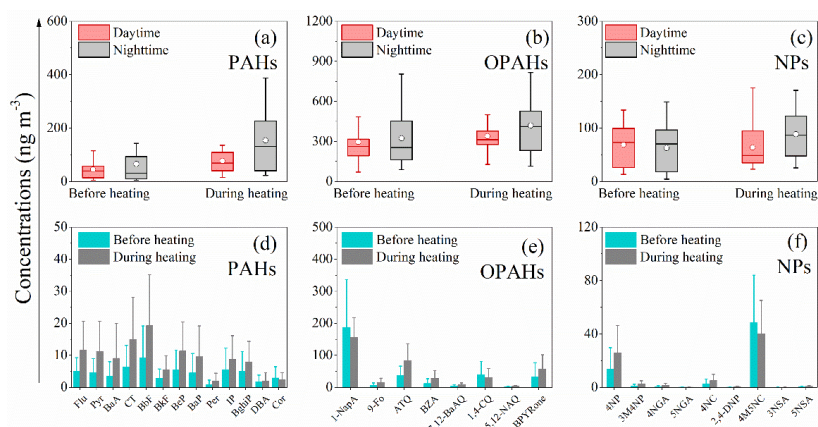
296

Fig.4 Time series of levoglucosan (a), PAHs(b), OPAHs (c), and NPs (d) in the autumn and winter of Dongying.

297

298

299



300

Fig.5 Diurnal variation and component concentrations of PAHs (a, d), OPAHs (b, e), and NPs (c, f) before and during heating. Markers represent mean values, while whiskers denote the 25th and 75th percentiles.

301

302

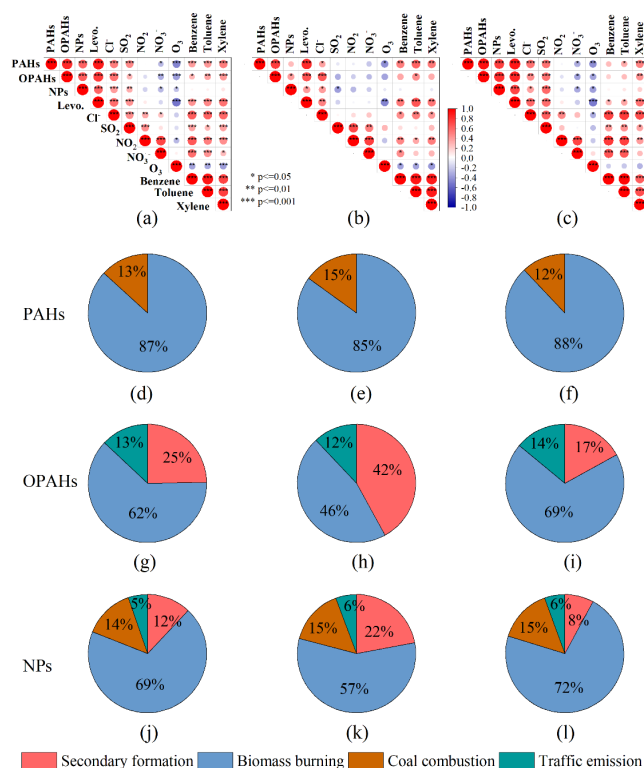
303



304 3.3 Source identification and quantitative analysis

305 3.3.1 Primary Sources of Key Pollutants

306 To better understand the primary influencing factors, Pearson correlation analyses
307 were conducted to analyze the relationships between OPAHs, PAHs, and NPs with key
308 PM_{2.5} components, gaseous pollutants, and VOC precursors. The results, presented in
309 Fig. 6a-c, include correlations with levoglucosan, Cl⁻, SO₂, NO₂, NO₃⁻, O₃, benzene,
310 toluene, and xylene. A substantial positive correlation was observed between OPAHs,
311 PAHs, and NPs, suggesting a common source or similar formation mechanisms,
312 particularly during the heating period. Furthermore, strong relationship was observed
313 between these aromatic compounds and primary pollutants throughout the sampling
314 campaign, such as levoglucosan ($r=0.84(p<0.001)$), 0.68 ($p<0.01$), 0.39 ($p<0.05$) for
315 PAHs, OPAHs, and NPs, respectively), and Cl⁻ ($r=0.36(p<0.05)$), 0.65 ($p<0.001$), 0.39
316 ($p<0.05$), respectively) (Fig. 6b). These relationships were strengthened during heating,
317 especially for SO₂ (Fig.6c). The data suggests that the levels of aromatic compounds
318 were substantially affected by burning emissions throughout the sampling period which
319 may be attributed to various sources such as biomass burning (Wang et al., 2017; Lin
320 et al., 2017; Chow et al., 2015) and coal combustion (Lu et al., 2019). Specifically,
321 biomass burning emerged as a major source of pollution throughout the entire campaign,
322 while the contribution mediated by coal combustion increased remarkably during the
323 heating period.



324

325 Fig.6 Correlations between PAHs, OPAHs, and NPs and key gas pollutants and
 326 aerosol components throughout the entire campaign (a), before heating (b), and during
 327 heating (c) (* $p < 0.05$, ** $p < 0.01$, *** $p < 0.001$); Source apportionments for PAHs (d,
 328 e, f), OPAHs (g, h, i), and NPs (j, k, l) during the whole campaign, before heating, and
 329 during heating, respectively; SF: secondary formation; FF: fossil fuel combustion;
 330 BB: biomass burning; CC: coal combustion; TE: traffic emission).

331 3.3.2 Source contribution

332 To further analyze the quantitative and qualitative effects of primary emissions as
 333 well as secondary formation, this study identified four categories of distinct sources
 334 during the campaign using the PMF model, as shown in Fig. S1. The first source factor,
 335 biomass burning, was recognized by the highest levoglucosan concentrations and
 336 increased particulate levels of K^+ and Cl^- within $PM_{2.5}$ (Fig. S1a). Biomass burning



337 emerged as the predominant source of aromatic compounds in the urban atmosphere of
338 Dongying during autumn and winter (Fig. 6d-l), contributing 87, 62, and 69% of the
339 total PAHs, OPAHs, and NPs, respectively, throughout the entire campaign (Fig.6d, g,
340 j). Moreover, the proportional contributions of burning biomass were also higher while
341 heating than before heating. A large number of PAHs, along with their derivatives,
342 originate from biomass combustion, as reported by various previously published studies
343 (Yhab et al., 2021; Chong et al., 2021; Bai et al., 2023; Li et al., 2022; Luo et al., 2021).
344 Several previous studies have also established that NPs are directly released during
345 biomass combustion and found emission factors over a range of 0.4 to 11.1 mg kg⁻¹
346 (Hoffmann et al., 2007; Iinuma et al., 2007; Wang et al., 2017b).

347 The second source factor was identified as coal combustion, having the highest
348 SO₂ concentration (Fig. S1b). The average contribution of coal combustion to PAHs
349 and NPs was determined as 13% and 14%, respectively (Fig.6d, j). Furthermore, there
350 were no significant changes to the relative contributions prior to and during the heating
351 phase. Previous research has indicated that coal combustion-related activities
352 significantly contribute to elevated levels of particulate PAHs and NPs, particularly
353 during the heating season. (Lu et al., 2019; Wang et al., 2018; Ren et al., 2023; Cai et
354 al., 2022; Luo et al., 2021).

355 In comparison to the other factor profiles, the third source factor, traffic emission,
356 showed a higher NO concentration loading in this factor profile (Fig. S1c). The average
357 contribution of traffic emissions to OPAHs throughout the entire campaign was 13%,
358 with no substantial variation in the percentage of emissions before and during heating



359 (14%). There was a minimal change in the contribution of traffic emissions to NPs both
360 before and during heating; on average, these emissions accounted for 6% of total NPs
361 during the campaign (Fig.6j-l). Previous studies have identified the traffic emission as
362 an essential source of OPAHs (Chong et al., 2021; Wang et al., 2022), and road traffic
363 as a primary contributor to NPs (Zhang et al., 2010; Ren et al., 2022). These differences
364 can be attributed to variations in energy use and industrial structures across different
365 cities.

366 Secondary formation, the fourth factor, displayed high concentrations of O₃ and a
367 relatively higher abundance of SO₄²⁻, NO₃⁻, and NH₄⁺ (Fig. S1d). Secondary formation
368 contributed an average of 25% of OPAHs throughout the whole campaign (Fig.6g- i).
369 It was the second-largest source, with a significantly higher contribution before heating
370 (42%) compared to during heating (17%). However, secondary formation contributed
371 12% of NPs throughout the whole campaign, with higher contributions before heating
372 (22%) (Fig.6j- l). The vital role of secondary formation in contributing to both OPAHs
373 and NPs agreed with recent studies (Ren et al., 2024; Ren et al., 2022). Previous
374 modeling and field studies also identified secondary formation as a significant NPs
375 source in the atmosphere (Yuan et al., 2016b; Mayorga et al., 2021; Xie et al., 2017).

376 **3.4 Secondary formation mechanism based on quantum chemical calculations**

377 Aromatic hydrocarbons are a major class of VOCs that play a vital role in the
378 production of secondary organic aerosols (SOA), particularly in urban areas (Song et
379 al., 2021). However, this study reported the positive correlation of these aromatic



380 compounds with the key precursors (i.e. benzene, toluene, xylene), while a negative
381 correlation with NO_2 , NO_3^- and O_3 , which are key parameters during the reaction
382 process (Fig.6a-c). Therefore, these substances were primarily derived from the same
383 source as the precursors, rather than their main products. Furthermore, considering the
384 substantial effect of biomass combustion, these compounds are probably the secondary
385 products formed through the oxidation process of gaseous pollutants released during
386 the biomass burning process. Nitroaromatic hydrocarbons are critical species in the
387 environment that are influenced by biomass combustion emissions. Phenol,
388 nitrobenzene, and *P*-Cresol are their significant precursors (Wang et al., 2020).
389 Therefore, to better comprehend the formation pathways of NPs, density functional
390 theory calculations at the M06-2X/6-311++G(2df,2p) level of theory were carried out
391 to explore the oxidation processes of major precursors by NO_2 and OH, specifically for
392 the dominant species 4NP and 4M5NC (Huang et al., 2010; Roman et al., 2022;
393 Shenghur et al., 2014; Wang et al., 2019b). Electronic energies (EDFT), Gibbs free
394 energies (GDFT) as well as the imaginary frequency of the reactant monomers, reactant
395 complexes (RC), transition states (TS), intermediate (IM) and product complexes (PC)
396 at 298.15 K and 1 atm were collected in Tables S1-S4 of the Supplementary Information.
397 The overall formation mechanisms, detailed in Fig. 7a, include both H-abstraction and
398 OH/ NO_2 addition steps where Mechanisms 1 and 2 show the two-step formation
399 pathways for 4NP, while Mechanism 3 describes the four-step pathway for 4M5NC.

400 In the H-abstraction step, either an OH radical or NO_2 molecule abstracts a
401 hydrogen atom from the aromatic ring, forming an intermediate free radical (IM) and



402 resulting in the formation of H₂O or HONO. In the OH/NO₂ addition step, the IMs react
403 with OH or NO₂ without any reaction barriers. In Table S1 of the Supplementary
404 Material, the calculated binding energy (E), Gibbs free energy change (ΔG) for the
405 reactant monomers, Gibbs free energy (G), transition states (TS), reactant complexes
406 (RC), intermediate (IM) and PCs are presented. While Fig.7b exhibited the calculated
407 dominant formation mechanism of 4NP and 4M5NC along with the reaction barrier in
408 kcal/mol.

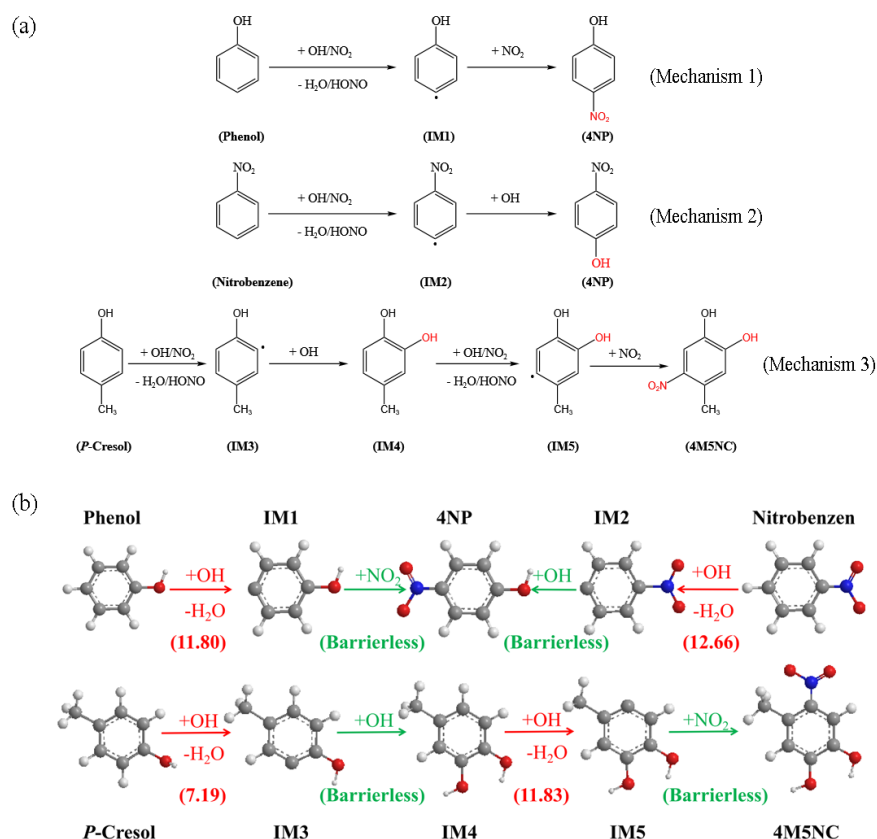
409 For the formation of 4NP, two precursors, phenol and nitrobenzene, were selected
410 which contain three distinct types of hydrogen atoms in their aromatic rings (*ortho*-,
411 *meta*-, and *para*-H). Here only the *para*-H is considered for the formation of 4NP.
412 During the daytime, when the gas-phase concentration of OH radicals is significant,
413 phenol initially reacts with OH to yield a reactant complex RC_{ph-OH} with a ΔG of 3.16
414 kcal/mol. Then RC_{ph} must overcome a reaction barrier of 8.64 kcal/mol to transition to
415 the TS_{ph-OH} state, resulting in the generation of IM1, a free radical intermediate with a
416 ΔG of -1.03 kcal/mol. The overall H-abstraction step was slightly exothermic, with a
417 reaction barrier of 11.80 kcal/mol. At nighttime, with a sharp decrease in OH
418 concentrations and a relatively higher level of NO₂, the daytime-generated IM1 rapidly
419 proceeded through a reaction with NO₂ that has no energy barrier, resulting in the
420 forming 4NP with a ΔG of -64.50 kcal/mol.

421 During nighttime, a parallel H-abstraction step occurred where NO₂, instead of
422 OH, abstracted a hydrogen atom from phenol. However, this step had high overall
423 reaction barriers, reaching 40.31 kcal/mol in the gas phase and 40.54 kcal/mol in the



424 liquid phase (water). Moreover, the reaction was highly endothermic with the ΔG of
425 36.51 and 36.45 kcal/mol in the gas phase and liquid phase, respectively, indicating that
426 the H-abstraction step initiated by NO_2 was not feasible. Therefore, the calculations for
427 Mechanisms 2 and 3 focused solely on the H-abstraction step initiated by OH.

428 For an alternative formation pathway of 4NP from nitrobenzene during the
429 daytime, the overall H-abstraction step was slightly exothermic (-1.08 kcal/mol) with a
430 reaction barrier of 12.66 kcal/mol. The generated IM2 then proceeded through a highly
431 exothermic and barrier-free OH addition step to form 4NP. In a comparative analysis,
432 it was possible to initiate 4NP formation with both phenol and nitrobenzene. For
433 mechanism 1, phenol was preferred to undergo the H-abstraction reaction during the
434 daytime and the NO_2 addition reaction at nighttime. For mechanism 2, nitrobenzene
435 preferred to undergo both reactions involving H-abstraction and OH addition during the
436 daytime.



437

438 Fig.7 (a) Suggested formation mechanism for 4NP and 4M5NC (b) The proposed
 439 dominant formation mechanism of 4NP and 4M5NC at the M06-2X/6-
 440 311++G(2df,2p) level of theory. H, C, S, N, and O atoms are depicted as white, gray,
 441 yellow, blue, and red spheres, respectively. The reaction barrier presented in the
 442 parentheses are given in kcal/mol.

443 The formation of 4M5NC followed a four-step mechanism with *p*-Cresol as the
 444 precursor. During the daytime, *p*-Cresol initially reacted with OH to form free radical
 445 intermediate IM3, overcoming a reaction barrier of 7.19 kcal/mol. After that, IM3
 446 underwent a highly exothermic OH addition step without any energy barrier to form
 447 IM4 which was then proceeded through a reaction barrier of 11.83 kcal/mol to produce
 448 IM5. At nighttime, the IM5 formed during the daytime quickly reacted through a highly
 449 exothermic NO₂ addition step with no significant energy barrier, resulting in the



450 formation of 4M5NC, with a ΔG of -61.14 kcal/mol in the gas phase and -63.47
451 kcal/mol in the liquid phase.

452 **4 Conclusions**

453 PAHs, OPAH, and NACs in the PM_{2.5} samples were analyzed during autumn and
454 winter in Dongying, a petrochemical industrial city. The concentrations of all these
455 species were significantly greater during the heating period in comparison to before
456 heating. Furthermore, these compounds demonstrated higher levels at night than during
457 the day, whereas NPs showed no notable diurnal variation. BbF, 1-NapA, and 4M5NC
458 were found to be the most abundant species for PAHs, OPAH, and NACs, respectively.
459 Biomass burning emerged as the primary source of aromatic compounds, particularly
460 during the heating period. Quantum chemical calculations revealed that the formation
461 mechanisms of 4NP and 4M5NC involve both H-abstraction and OH/NO₂ addition
462 steps with the H-abstraction step serving as the rate-limiting step, while the OH/NO₂
463 addition step proceeded without an energy barrier. Phenol and *P*-Cresol were
464 determined as the primary precursors for the formation of 4NP and 4M5NC,
465 respectively. This study offers the first detailed investigation into the sources and
466 forming mechanisms of aromatic compounds in the atmosphere of petrochemical cities
467 in the Yellow River Delta. It offers essential data and strategic guidance for reducing
468 aromatic compound emissions in such urban environments.



469 **Data availability**

470 The Data used in this study are available from the first author upon request (Yanqin
471 Ren via renyq@craes.org.cn).

472 **Author contributions**

473 YR, GW and YJ designed the research; YJ, FB and ZW collected the samples and
474 analyzed the data; YR and HZ wrote the manuscript; JL, RG, FL, ZL and HL
475 contributed to the paper with useful scientific discussions and comments.

476 **Competing interests**

477 The contact author has declared that none of the authors has any competing
478 interests.

479 **Acknowledgements**

480 We are grateful to Mr. Xiaoyu Yan and Ms. Xurong Bai from Chinese Research
481 Academy of Environmental Sciences for their help in collecting samples, and Mr.
482 Yubao Chen and his colleagues from East China Normal University for providing help
483 with analytical testing.



484 **Financial support**

485 This research was supported by the National Research Program for Key Issues in
486 Air Pollution Control (No. DQGG202121, DQGG2021301), Key Technologies
487 Research and Development Program (No. 2023YFC3706105), Fundamental Research
488 Funds for Central Public Welfare Scientific Research Institutes of China (No.
489 2019YSKY-018), and the National Natural Science Foundation of China (No.
490 42130704; No. 41907197; No.22306179).

491

492 **References**

- 493 Alves, C., Vicente, A., Custódio, D., Cerqueira, M., Nunes, T., Pio, C., Lucarelli, F., Calzolari, G., Nava,
494 S., and Diapouli, E.: Polycyclic aromatic hydrocarbons and their derivatives (nitro-PAHs,
495 oxygenated PAHs, and azaarenes) in PM_{2.5} from Southern European cities, *Sci. Total. Environ.*,
496 595, 494-504, <https://dx.doi.org/10.1016/j.scitotenv.2017.03.256>, 2017.
- 497 Bai, X., Wei, J., Ren, Y., Gao, R., Chai, F., Li, H., Xu, F., and Kong, Y.: Pollution characteristics and
498 health risk assessment of Polycyclic aromatic hydrocarbons and Nitrated polycyclic aromatic
499 hydrocarbons during heating season in Beijing, *JEnvS*, 123, 169-182,
500 <https://doi.org/10.1016/j.jes.2022.02.047>, 2023.
- 501 Bandowe, B. A. M., Lueso, M. G., and Wilcke, W.: Oxygenated polycyclic aromatic hydrocarbons and
502 azaarenes in urban soils: A comparison of a tropical city (Bangkok) with two temperate cities
503 (Bratislava and Gothenburg), *Chemosphere*, 107, 407-414,
504 <https://dx.doi.org/10.1016/j.chemosphere.2014.01.017>, 2014.
- 505 Bandowe, B. A. M., Shukurov, N., Kersten, M., and Wilcke, W.: Polycyclic aromatic hydrocarbons
506 (PAHs) and their oxygen-containing derivatives (OPAHs) in soils from the Angren industrial area,
507 Uzbekistan, *Environ. Pollut.*, 158, 2888-2899, <https://doi.org/10.1016/j.envpol.2010.06.012>,
508 2010.
- 509 Bolton, J. L., Trush, M. A., Penning, T. M., Dryhurst, G., and Monks, T. J.: Role of quinones in toxicology,
510 *Chem. Res. Toxicol.*, 13, 135-160, <https://doi.org/10.1021/tx9902082>, 2000.
- 511 Booth, A. M., Murphy, B., Riipinen, I., Percival, C. J., and Topping, D. O.: Connecting Bulk Viscosity
512 Measurements to Kinetic Limitations on Attaining Equilibrium for a Model Aerosol Composition,
513 *EnST*, 48, 9298-9305, <https://doi.org/10.1021/es501705c>, 2014.
- 514 Cai, D., Wang, X., George, C., Cheng, T., Herrmann, H., Li, X., and Chen, J.: Formation of Secondary
515 Nitroaromatic Compounds in Polluted Urban Environments, *J. Geophys. Res.-Atmos.*, 127,



- 516 <https://doi.org/10.1029/2021JD036167>, 2022.
- 517 Chen, L., Liu, W., Tao, S., and Liu, W.: Spatiotemporal variations and source identification of
518 atmospheric nitrated and oxygenated polycyclic aromatic hydrocarbons in the coastal cities of the
519 Bohai and Yellow seas in northern China, *Chemosphere*, 279, 130565,
520 <http://doi.org/10.1016/j.chemosphere.2021.130565>, 2021.
- 521 Chen, T., Xue, L., Zheng, P., Zhang, Y., Liu, Y., Sun, J., Han, G., Li, H., Zhang, X., Li, Y., Li, H., Dong,
522 C., Xu, F., Zhang, Q., and Wang, W.: Volatile organic compounds and ozone air pollution in an oil
523 production region in northern China, *Atmos. Chem. Phys.*, 20, 7069-7086,
524 <https://doi.org/10.5194/acp-20-7069-2020>, 2020.
- 525 Chen, Y., Sheng, G., Bi, X., Feng, Y., Mai, B., and Fu, J.: Emission factors for carbonaceous particles
526 and polycyclic aromatic hydrocarbons from residential coal combustion in China, *Environ. Sci.*
527 *Technol.*, 39, 1861-1867, <https://doi.org/10.1021/es0493650>, 2005.
- 528 Chong, W., Bambc, D., Yha, E., Jc, A., F, J., F, J., and Ww, G.: Polycyclic aromatic compounds (PAHs,
529 oxygenated PAHs, nitrated PAHs, and azaarenes) in air from four climate zones of China:
530 Occurrence, gas/particle partitioning, and health risks, *Sci. Total. Environ.*, 786, 147234,
531 <https://doi.org/10.1016/j.scitotenv.2021.147234>, 2021.
- 532 Chow, K. S., Huang, X. H. H., and Yu, J. Z.: Quantification of nitroaromatic compounds in atmospheric
533 fine particulate matter in Hong Kong over 3 years: field measurement evidence for secondary
534 formation derived from biomass burning emissions, *Environmental Chemistry*, 13, 665-673,
535 <https://doi.org/10.1071/EN15174>, 2015.
- 536 Chung, M. Y., Lazaro, R. A., Lim, D., Jackson, J., Lyon, J., Rendulic, D., and Hasson, A. S.: Aerosol-
537 borne quinones and reactive oxygen species generation by particulate matter extracts, *Environ.*
538 *Sci. Technol.*, 40, 4880-4886, <https://doi.org/10.1021/es0515957>, 2006.
- 539 del Rosario Sierra, M., Rosazza, N. G., and Préndez, M.: Polycyclic aromatic hydrocarbons and their
540 molecular diagnostic ratios in urban atmospheric respirable particulate matter, *Atmos. Res.*, 75,
541 267-281, <https://doi.org/10.1016/j.atmosres.2005.01.003>, 2005.
- 542 Elzein, A., Dunmore, R. E., Ward, M. W., Hamilton, J. F., and Lewis, A. C.: Variability of polycyclic
543 aromatic hydrocarbons and their oxidative derivatives in wintertime Beijing, China, *Atmos. Chem.*
544 *Phys.*, 19, 8741-8758, <https://doi.org/10.5194/acp-19-8741-2019>, 2019.
- 545 Gonzalez, C. and Schlegel, H. B.: An improved algorithm for reaction path following, *The Journal of*
546 *Chemical Physics*, 90, 2154-2161, <http://doi.org/10.1063/1.456010>, 1989.
- 547 Harrison, M. A. J., Barra, S., Borghesi, D., Vione, D., Arsene, C., and Olariu, R. I.: Nitrated phenols in
548 the atmosphere: a review, *Atmos. Environ.*, 39, 231-248,
549 <https://doi.org/10.1016/j.atmosenv.2004.09.044>, 2005.
- 550 Huang, M., Wang, Z., Hao, L., and Zhang, W.: Theoretical investigation on the mechanism and kinetics
551 of OH radical with ethylbenzene, *IJQC*, 111, 3125-3134, <http://doi.org/10.1002/qua.22751>, 2010.
- 552 Jakober, C. A., Riddle, S. G., Robert, M. A., Destailats, H., Charles, M. J., Green, P. G., and Kleeman,
553 M. J.: Quinone emissions from gasoline and diesel motor vehicles, *Environ. Sci. Technol.*, 41,
554 4548-4554, <https://doi.org/10.1021/es062967u>, 2007.
- 555 Kahnt, A., Behrouzi, S., Vermeylen, R., Shalamzari, M. S., Vercauteren, J., Roekens, E., Claeys, M., and
556 Maenhaut, W.: One-year study of nitro-organic compounds and their relation to wood burning in
557 PM10 aerosol from a rural site in Belgium, *Atmos. Environ.*, 81, 561-568,
558 <https://dx.doi.org/10.1016/j.atmosenv.2013.09.041>, 2013.
- 559 Kashiwakura, K. and Sakamoto, K.: Emission Characteristics and Cancer Risks of Polycyclic Aromatic



- 560 Hydrocarbon Emissions from Diesel-fueled Vehicles Complying with Recent Regulations, J.
561 Health Sci., 56, 200-207, <https://doi.org/10.1248/jhs.56.200>, 2010.
- 562 Kitanovski, Z., Shahpoury, P., Samara, C., Voliotis, A., and Lammel, G.: Composition and mass size
563 distribution of nitrated and oxygenated aromatic compounds in ambient particulate matter from
564 southern and central Europe – implications for the origin, Atmos. Chem. Phys., 20, 2471-2487,
565 <https://doi.org/10.5194/acp-20-2471-2020>, 2020.
- 566 Lammel, G., Kitanovski, Z., Kukucka, P., Novák, J., and Wietzoreck, M.: Oxygenated and nitrated
567 polycyclic aromatic hydrocarbons (OPAHs, NPAHs) in ambient air - levels, phase partitioning,
568 mass size distributions and inhalation bioaccessibility, Environ. Sci. Technol., 54, 2615-2625,
569 <https://dx.doi.org/10.1021/acs.est.9b06820>, 2020.
- 570 Li, J. J., Wang, G. H., Wang, X. M., Cao, J. J., Sun, T., Cheng, C. L., Meng, J. J., Hu, T. F., and Liu, S.
571 X.: Abundance, composition and source of atmospheric PM_{2.5} at a remote site in the Tibetan
572 Plateau, China, Tellus B., 65, 20281, <https://doi.org/10.3402/tellusb.v65i0.20281>, 2013.
- 573 Li, X., Yang, Y., Liu, S., Zhao, Q., Wang, G., and Wang, Y.: Light absorption properties of brown carbon
574 (BrC) in autumn and winter in Beijing: Composition, formation and contribution of nitrated
575 aromatic compounds, Atmos. Environ., 223, 117289,
576 <https://doi.org/10.1016/j.atmosenv.2020.117289>, 2020.
- 577 Li, Y. and Wang, L.: The atmospheric oxidation mechanism of 1,2,4-trimethylbenzene initiated by OH
578 radicals, PCCP, 16, <http://doi.org/10.1039/c4cp02027h>, 2014.
- 579 Li, Y., Bai, X., Ren, Y., Gao, R., Ji, Y., Wang, Y., and Li, H.: PAHs and nitro-PAHs in urban Beijing from
580 2017 to 2018: Characteristics, sources, transformation mechanism and risk assessment, J. Hazard.
581 Mater., 436, 1-11, <https://doi.org/10.1016/j.jhazmat.2022.129143>, 2022.
- 582 Liang, Y., Wang, X., Dong, S., Liu, Z., Mu, J., Lu, C., Zhang, J., Li, M., Xue, L., and Wang, W.: Size
583 distributions of nitrated phenols in winter at a coastal site in north China and the impacts from
584 primary sources and secondary formation, Chemosphere, 250, 126256,
585 <https://doi.org/10.1016/j.chemosphere.2020.126256>, 2020.
- 586 Lin, P., Bluvshstein, N., Rudich, Y., Nizkorodov, S. A., Laskin, J., and Laskin, A.: Molecular Chemistry
587 of Atmospheric Brown Carbon Inferred from a Nationwide Biomass Burning Event, Environ. Sci.
588 Technol., 51, 11561-11570, <https://doi.org/10.1021/acs.est.7b02276>, 2017.
- 589 Lin, P., Liu, J., Shilling, J. E., Kathmann, S. M., Laskin, J., and Laskin, A.: Molecular characterization
590 of brown carbon (BrC) chromophores in secondary organic aerosol generated from photo-
591 oxidation of toluene, PCCP, 17, 23312-23325, <https://doi.org/10.1039/c5cp02563j>, 2015a.
- 592 Lin, Y., Ma, Y., Qiu, X., Li, R., Fang, Y., Wang, J., Zhu, Y., and Hu, D.: Sources, transformation, and
593 health implications of PAHs and their nitrated, hydroxylated, and oxygenated derivatives in PM_{2.5}
594 in Beijing, J. Geophys. Res.-Atmos., 120, 7219-7228, <https://doi.org/10.1002/2015JD023628>,
595 2015b.
- 596 Lu, C., Wang, X., Li, R., Gu, R., Zhang, Y., Li, W., Gao, R., Chen, B., Xue, L., and Wang, W.: Emissions
597 of fine particulate nitrated phenols from residential coal combustion in China, Atmos. Environ.,
598 203, 10-17, <https://doi.org/10.1016/j.atmosenv.2019.01.047>, 2019.
- 599 Lu, C., Wang, X., Zhang, J., Liu, Z., Liang, Y., Dong, S., Li, M., Chen, J., Chen, H., Xie, H., Xue, L.,
600 and Wang, W.: Substantial emissions of nitrated aromatic compounds in the particle and gas
601 phases in the waste gases from eight industries, Environ. Pollut., 283, 117132,
602 <https://doi.org/10.1016/j.envpol.2021.117132>, 2021.
- 603 Luo, M., Ji, Y., Ren, Y., Gao, F., Zhang, H., Zhang, L., Yu, Y., and Li, H.: Characteristics and Health Risk



- 604 Assessment of PM_{2.5}-Bound PAHs during Heavy Air Pollution Episodes in Winter in Urban Area
605 of Beijing, China, *Atmos*, 12, <https://doi.org/10.3390/atmos12030323>, 2021.
- 606 Ma, L., Li, B., Liu, Y., Sun, X., Fu, D., Sun, S., Thapa, S., Geng, J., Qi, H., Zhang, A., and Tian, C.:
607 Characterization, sources and risk assessment of PM_{2.5}-bound polycyclic aromatic hydrocarbons
608 (PAHs) and nitrated PAHs (NPAHs) in Harbin, a cold city in Northern China, *Journal of Cleaner
609 Production*, 264, <https://doi.org/10.1016/j.jclepro.2020.121673>, 2020.
- 610 Mayorga, R. J., Zhao, Z., and Zhang, H.: Formation of secondary organic aerosol from nitrate radical
611 oxidation of phenolic VOCs: Implications for nitration mechanisms and brown carbon formation,
612 *Atmos. Environ.*, 244, <https://doi.org/10.1016/j.atmosenv.2020.117910>, 2021.
- 613 Mohr, C., Lopez-Hilfiker, F. D., Zotter, P., A. S. H. P., Xu, L., Ng, N. L., Herndon, S. C., Williams, L.
614 R., Franklin, J. P., Zahniser, M. S., Worsnop, D. R., Knighton, W. B., Aiken, A. C., Gorkowski, K.
615 J., Dubey, M. K., Allan, J. D., and Thornton, J. A.: Contribution of Nitrated Phenols to Wood
616 Burning Brown Carbon Light Absorption in Detling, United Kingdom during Winter Time,
617 *Environ. Sci. Technol.*, 47, 6316-6324, <https://doi.org/10.1021/es400683v>, 2013.
- 618 Oda, J., Nomura, S., Yasuhara, A., and Shibamoto, T.: Mobile sources of atmospheric polycyclic aromatic
619 hydrocarbons in a roadway tunnel, *Atmos. Environ.*, 35, 4819-4827,
620 [https://doi.org/10.1016/S1352-2310\(01\)00262-X](https://doi.org/10.1016/S1352-2310(01)00262-X), 2001.
- 621 Pedersen, D. U., Durant, J. L., Taghizadeh, K., Hemond, H. F., Lafleur, A. L., and Cass, G. R.: Human
622 cell mutagens in respirable airborne particles from the northeastern United States. 2.
623 Quantification of mutagens and other organic compounds, *Environ. Sci. Technol.*, 39, 9547-9560,
624 <https://doi.org/10.1021/es050886c> 2005.
- 625 Peng, B., Dong, Q., Li, F., Wang, T., Qiu, X., and Zhu, T.: A systematic review of polycyclic aromatic
626 hydrocarbon derivatives: occurrences, levels, biotransformation, exposure biomarkers, and
627 toxicity, *Environmental Science & Technology*, 57, 15314-15335,
628 <https://doi.org/10.1021/acs.est.3c03170>, 2023.
- 629 Ren, Y., Wang, G., Wei, J., Tao, J., Zhang, Z., and Li, H.: Contributions of primary emissions and
630 secondary formation to nitrated aromatic compounds in themountain background region of
631 Southeast China, *Atmos. Chem. Phys.*, 23, 6835-6848, <https://doi.org/10.5194/acp-23-6835-2023>,
632 2023.
- 633 Ren, Y., Wei, J., Wang, G., Wu, Z., Ji, Y., and Li, H.: Evolution of aerosol chemistry in Beijing under
634 strong influence of anthropogenic pollutants: Composition, sources, and secondary formation of
635 fine particulate nitrated aromatic compounds, *Environ. Res.*, 204, 111982,
636 <https://doi.org/10.1016/j.envres.2021.111982>, 2022.
- 637 Ren, Y., Wei, J., Wu, Z., Ji, Y., Bi, F., Gao, R., Wang, X., Wang, G., and Li, H.: Chemical components
638 and source identification of PM_{2.5} in non-heating season in Beijing: The influences of biomass
639 burning and dust, *Atmos. Res.*, 105412, <https://doi.org/10.1016/j.atmosres.2020.105412>, 2021.
- 640 Ren, Y., Wu, Z., Ji, Y., Bi, F., Li, J., Zhang, H., Zhang, H., Li, H., and Wang, G.: Non-negligible secondary
641 contribution to brown carbon in autumn and winter: inspiration from particulate nitrated and
642 oxygenated aromatic compounds in urban Beijing, *Atmos. Chem. Phys.*, 24, 6525-6538,
643 <https://doi.org/10.5194/acp-24-6525-2024>, 2024.
- 644 Ren, Y., Zhou, B., Tao, J., Cao, J., Zhang, Z., Wu, C., Wang, J., Li, J., Zhang, L., Han, Y., Liu, L., Cao,
645 C., and Wang, G.: Composition and size distribution of airborne particulate PAHs and oxygenated
646 PAHs in two Chinese megacities, *Atmos. Res.*, 183, 322-330,
647 <https://doi.org/10.1016/j.atmosres.2020.105412>, 2017.



- 648 Roman, C., Arsene, C., Bejan, I. G., and Olariu, R. I.: Investigations into the gas-phase photolysis and
649 OH radical kinetics of nitrocatechols: implications of intramolecular interactions on their
650 atmospheric behaviour, *Atmos. Chem. Phys.*, 22, 2203-2219, [https://doi.org/10.5194/acp-22-2203-](https://doi.org/10.5194/acp-22-2203-2022)
651 [2022](https://doi.org/10.5194/acp-22-2203-2022), 2022.
- 652 Sarigiannis, D. A., Karakitsios, S. P., Dimitrios, Z., Spyridoula, N., and Marianthi, K.: Lung cancer risk
653 from PAHs emitted from biomass combustion, *Environ. Res.*, 137, 147-156,
654 <https://dx.doi.org/10.1016/j.envres.2014.12.009>, 2015.
- 655 Shen, G., Yang, Y., Wang, W., Tao, S., Zhu, C., Min, Y., Xue, M., Ding, J., Wang, B., and Wang, R.:
656 Emission factors of particulate matter and elemental carbon for crop residues and coals burned in
657 typical household stoves in China, *Environ. Sci. Technol.*, 44, 7157-7162,
658 <https://doi.org/10.1021/es101313y>, 2010.
- 659 Shenghur, A., Weber, K. H., Nguyen, N. D., Sontising, W., and Tao, F.-M.: Theoretical Study of the
660 Hydrogen Abstraction of Substituted Phenols by Nitrogen Dioxide as a Source of HONO, *The*
661 *Journal of Physical Chemistry A*, 118, 11002-11014, <http://doi.org/10.1021/jp508516c>, 2014.
- 662 Song, M., Liu, Y., Li, X., and Lu, S.: Advances on Atmospheric Oxidation Mechanism of Typical
663 Aromatic Hydrocarbons, *Acta Chim. Sinica*, 79, 1214-1231, <https://doi.org/10.6023/a21050224>,
664 2021.
- 665 Takano, Y. and Houk, K. N.: Benchmarking the Conductor-like Polarizable Continuum Model (CPCM)
666 for Aqueous Solvation Free Energies of Neutral and Ionic Organic Molecules, *Journal of*
667 *Chemical Theory and Computation*, 1, 70-77, <http://doi.org/10.1021/ct049977a>, 2005.
- 668 Teich, M., Van Pinxteren, D., Wang, M., Kecorius, S., Wang, Z., Müller, T., Mocnik, G., and Herrmann,
669 H.: Contributions of nitrated aromatic compounds to the light absorption of water-soluble and
670 particulate brown carbon in different atmospheric environments in Germany and China, *Atmos.*
671 *Chem. Phys.*, 17, 1653-1672, <https://doi.org/10.5194/acp-17-1653-2017>, 2017.
- 672 Wang, L., Wang, X., Gu, R., Hao, W., and Wang, W.: Observations of fine particulate nitrated phenols in
673 four sites in northern China: concentrations, source apportionment, and secondary formation,
674 *Atmos. Chem. Phys.*, 18, 4349-4359, <https://doi.org/10.5194/acp-18-4349-2018>, 2018.
- 675 Wang, L., Dong, S., Liu, M., Tao, W., Xiao, B., Zhang, S., Zhang, P., and Li, X.: Polycyclic aromatic
676 hydrocarbons in atmospheric PM_{2.5} and PM₁₀ in the semi-arid city of Xi'an, Northwest China:
677 Seasonal variations, sources, health risks, and relationships with meteorological factors, *Atmos.*
678 *Res.*, 229, 60-73, <https://doi.org/10.1016/j.atmosres.2019.06.014>, 2019a.
- 679 Wang, T., Zhao, J., Liu, Y., Peng, J., Wu, L., and Mao, H.: PM_{2.5}-Bound Polycyclic Aromatic
680 Hydrocarbons (PAHs), Nitrated PAHs (NPAHs) and Oxygenated PAHs (OPAHs) in Typical
681 Traffic-Related Receptor Environments, *Journal of Geophysical Research, D. Atmospheres*, 127,
682 e2021JD035951, <https://doi.org/10.1029/2021JD035951>, 2022.
- 683 Wang, W., Jariyasopit, N., Schrlau, J., Jia, Y., Tao, S., Yu, T.-W., Dashwood, R. H., Zhang, W., Wang, X.,
684 and Simonich, S. L. M.: Concentration and photochemistry of PAHs, NPAHs, and OPAHs and
685 toxicity of PM_{2.5} during the Beijing Olympic Games, *Environ. Sci. Technol.*, 45, 6887-6895,
686 <http://dx.doi.org/10.1021/es201443z>, 2011.
- 687 Wang, X., Gu, R., Wang, L., Xu, W., Zhang, Y., Chen, B., Li, W., Xue, L., Chen, J., and Wang, W.:
688 Emissions of fine particulate nitrated phenols from the burning of five common types of biomass,
689 *Environ. Pollut.*, 230, 405-412, <http://dx.doi.org/10.1016/j.envpol.2017.06.072>, 2017.
- 690 Wang, Y., Hu, M., Li, X., and Xu, N.: Chemical Composition, Sources and Formation Mechanisms of
691 Particulate Brown Carbon in the Atmosphere (in Chinese), *Progress in Chemistry*, 32, 627-645,



- 692 <http://doi.org/10.7536/PC190917>, 2020.
- 693 Wang, Y., Hu, M., Wang, Y., Zheng, J., Shang, D., Yang, Y., Liu, Y., Li, X., Tang, R., Zhu, W., Du, Z.,
694 Wu, Y., Guo, S., Wu, Z., Lou, S., Hallquist, M., and Yu, J. Z.: The formation of nitro-aromatic
695 compounds under high NO₂ and anthropogenic VOC
696 conditions in urban Beijing, China, *Atmos. Chem. Phys.*, 19, 7649-7665,
697 <http://doi.org/10.5194/acp-19-7649-2019>, 2019b.
- 698 Wu, C., Wang, G., Li, J., Li, J., Cao, C., Ge, S., Xie, Y., Chen, J., Li, X., Xue, G., Wang, X., Zhao, Z.,
699 and Cao, F.: The characteristics of atmospheric brown carbon in Xi'an, inland China: sources, size
700 distributions and optical properties, *Atmos. Chem. Phys.*, 20, 2017-2030,
701 <https://doi.org/10.5194/acp-20-2017-2020>, 2020.
- 702 Xie, M., Chen, X., Hays, M. D., Lewandowski, M., Offenberg, J. H., Kleindienst, T. E., and Holder, A.
703 L.: Light Absorption of Secondary Organic Aerosol: Composition and Contribution of
704 Nitroaromatic Compounds, *Environ. Sci. Technol.*, 51, 11607-11616,
705 <https://doi.org/10.1021/acs.est.7b03263>, 2017.
- 706 Yhab, D., Xxab, C., Dan, L. E., Xjab, C., Zha, B., Yca, B., Lxa, B., Mla, B., Hong, W. G., and Han, Z.:
707 Air pollution increases human health risks of PM 2.5-bound PAHs and nitro-PAHs: a case study
708 in the Yangtze River Delta, China, *Sci. Total. Environ.*, 770, 145402,
709 <https://doi.org/10.1016/j.scitotenv.2021.145402>, 2021.
- 710 Yuan, B., Liggió, J., Wentzell, J., Li, S. M., and Stark, H.: Secondary formation of nitrated phenols:
711 insights from observations during the Uintah Basin Winter Ozone Study (UBWOS) 2014, *Atmos.*
712 *Chem. Phys.*, 16, 2139-2153, <http://doi.org/10.5194/acp-16-2139-2016>, 2016a.
- 713 Yuan, B., Liggió, J., Wentzell, J., Li, S. M., and Stark, H.: Secondary formation of nitrated phenols:
714 insights from observations during the Uintah Basin Winter Ozone Study (UBWOS) 2014, *Atmos.*
715 *Chem. Phys.*, <https://doi.org/10.5194/acp-16-2139-2016>, 2016b.
- 716 Zhang, J., Yang, L., Mellouki, A., Chen, J., Chen, X., Gao, Y., Jiang, P., Li, Y., Yu, H., and Wang, W.:
717 Diurnal concentrations, sources, and cancer risk assessments of PM_{2.5}-bound PAHs, NPAHs, and
718 OPAHs in urban, marine and mountain environments, *Chemosphere*, 209, 147-155,
719 <https://doi.org/10.1016/j.chemosphere.2018.06.054>, 2018.
- 720 Zhang, Y. Y., Müller, L., Winterhalter, R., Moortgat, G. K., Hoffmann, T., and Poschl, U.: Seasonal cycle
721 and temperature dependence of pinene oxidation products, dicarboxylic acids and nitrophenols in
722 fine and coarse air particulate matter, *Atmos. Chem. Phys.*, 10, 7859 – 7873,
723 <https://doi.org/10.5194/acp-10-7859-2010>, 2010.
- 724 Zhao, Y. and Truhlar, D. G.: The M06 suite of density functionals for main group thermochemistry,
725 thermochemical kinetics, noncovalent interactions, excited states, and transition elements: two
726 new functionals and systematic testing of four M06-class functionals and 12 other functionals,
727 *Theor. Chem. Acc.*, 120, 215-241, <http://doi.org/10.1007/s00214-007-0310-x>, 2007.
- 728